A study on the structure and vibrations of diphenylamine by resonance-enhanced multiphoton ionization spectroscopy and *ab initio* calculations

Maarten G. H. Boogaarts, Gert von Helden, and Gerard Meijer
Department of Molecular and Laser Physics, University of Nijmegen, Toernooiveld, 6525 ED Nijmegen, The Netherlands

Laser-desorption jet-cooling has been applied in combination with mass-selective gas-phase spectroscopic techniques to study the structure and low-frequency vibrations of diphenylamine (DPA). Two-color $(1+1')$ resonance-enhanced multiphoton ionization has been used to measure the vibrationally resolved excitation spectrum of the $S_1 \leftarrow S_0$ transition in the 305–309 nm region. Ion-dip measurements have been performed to determine the vibrational structure in the electronic ground state. The electronic spectra of DPA are dominated by long progressions in low-frequency vibrations involving the motion of the phenyl rings as a whole. For the interpretation of the experimental data *ab initio* calculations have been performed at the Hartree–Fock level for the S_0-state and using single-excitation configuration interaction for the S_1-state. The DPA molecule is found to change from a pyramidal geometry around the N-atom with unequal torsional angles of the phenyl groups in the S_0-state to a planar geometry with equal torsional angles in the S_1-state. The two most prominent vibrational motions are the in-phase wagging and the in-phase torsion of the phenyl rings. In addition, the resonance-enhanced multiphoton ionization spectra of the $S_1 \leftarrow S_0$ transition in the DPA-Ar, DPA-Kr, and DPA-Xe van der Waals complexes have been measured. From these spectra it is inferred that there is a coupling between the van der Waals modes and the low-frequency intra-molecular modes of DPA. © *1996 American Institute of Physics.* [S0021-9606(96)01743-6]

I. INTRODUCTION

In the last few decades there has been a considerable interest in the determination of the structural and dynamical properties of bridged biphenylic molecules $(C_6H_5)_2X$ like diphenylether (X=O), diphenyl-sulfide (X=S), benzophenone (X=CO), biphenyl (X=), stilbene (X=CH=CH), diphenylamine (X=NH), and many others.[1–11] The attention mainly focussed on the equilibrium orientation of the phenyl rings, i.e., the twist angles of the phenyl groups around the C-X bonds relative to the C-X-C plane, and on the frequencies of the corresponding torsional motions. These properties are believed to play an important role in the intra-molecular dynamics as well as in the chemical behaviour of such molecules.

The orientation of the rings is dictated by the competition between two effects: the steric repulsion of the rings and the desired conjugation of the electronic π systems on the rings, either directly, or mediated through a lone pair orbital on X. There is a strong relationship between the molecular geometry and the nature of electronic transitions, and Huber and co-workers concluded from an extensive study on a series of aromatic amines, whose molecular configurations gradually change from a distinctly nonplanar to a planar geometry, that ''the excited state behaviour of aromatic amines is dominated by the influence of molecular geometry on spin-orbit coupling''.[3–6] The molecular geometry thereby also influences intersystem crossing (ISC) processes. In addition, the torsional modes are expected to determine intra-molecular vibrational relaxation (IVR). This has been inves-tigated in several studies on the low-frequency vibrations of benzophenone.[7–9]

Experimental studies on bridged biphenylic systems have often been backed by empirical and/or semi-empirical calculations.[4,9–13] However, drastic assumptions on the molecular geometry have usually been made. For example C_2 or C_{2v} symmetry of the molecule and planarity of the phenyl rings is often assumed. Predictions made from those calculations will fail for the aromatic amines, where the geometry around the N-nucleus is expected to be pyramidal due to a sp^3 electronic configuration.

More recently there has been a renewed interest in determining the geometrical, vibrational, and electronic structure of diphenylamine (DPA) and its derivatives in connection with the design and synthesis of organic ferromagnets, where polymer skeletons derived from poly-aniline are believed to be good candidates.[14,15] Ito *et al.* were the first to use *ab initio* molecular orbital methods to calculate the electronic structure of DPA and some of its derivatives. They investigated the relative energies of four predefined molecular conformations, but did not perform a full geometry optimization.[15]

Existing experimental data on DPA come from studies in the liquid or solid state.[1–6,16–20] Nonetheless, information pertaining to the geometry and dynamics of DPA and other bridged biphenylic molecules $(C_6H_5)_2X$ is surprisingly incomplete. Those properties are best studied in the gas phase on the isolated molecule. However, the vapour absorption spectra of these molecules are usually very broad due to

spectral congestion. This congestion can be removed by cooling the molecules in a supersonic expansion,[21,22] but molecular beam techniques have long been restricted to molecules with a sufficiently high vapour pressure that seeding of the sample molecules in a carrier gas can be performed. Many large organic molecules do not meet this requirement, and detailed gas-phase spectroscopic information on diphenylamine has been lacking for this reason. Optical spectra of DPA have been measured before in laser-desorption jet-cooling studies.[23–25] Although these studies did not aim at a detailed analysis of the DPA spectra, long progressions in low-frequency vibrational modes were reported in the electronic excitation spectra. It was concluded that the isolated molecule in the gas phase is rather floppy, and that the long progressions are indicative of a large change in the equilibrium geometry of the molecule upon excitation.

In this paper we report the vibrationally resolved electronic spectroscopy of diphenylamine, performed in a laser desorption jet cooling molecular beam spectrometer. Two kinds of measurements have been performed in this study: excitation spectroscopy to probe the vibrational levels in the first electronically excited singlet state S_1, and ion-dip spectroscopy to probe the vibrational levels in the ground state S_0. To facilitate the vibrational analysis of the DPA spectrum, also the spectrum of the deuterated species, i.e., a DPA molecule with the amine proton substituted by a D-atom, has been measured. In addition, measurements have been performed on van der Waals complexes of DPA with the rare gas atoms Ar, Kr, and Xe. The interpretation of the experimental data in terms of the geometry and the normal modes of DPA in both S_0 and S_1-state is backed by *ab initio* calculations. These calculations include a full geometry optimization, a normal mode analysis, and a calculation of the vibrational frequencies in both states.

II. EXPERIMENT

The laser desorption jet cooling mass spectrometer will be described in detail elsewhere,[26] and only a brief description will be given here. A scheme of the apparatus is depicted in Fig. 1. DPA is deposited in a piece of active carbon (Norit, R 2030) by solving DPA in an organic solvent (e.g., toluene) and soaking the charcoal piece in this solution. The charcoal is then dried and its surface is disposed of the overspill of DPA. The charcoal piece is positioned near the orifice of a pulsed jet expansion, where the unfocussed frequency-doubled output of a Nd:YAG laser (Spectra-Physics, GCR-11) is used for desorbing DPA from the charcoal matrix at an optimum laser fluence of $8 \cdot 10^6$ W/cm^2. The pulsed valve (R. M. Jordan Co.) is operated at a 10 Hz repetition rate with 2 bar backing pressure of the carrier gas. It releases gas pulses of typically 30 μs duration that expand through the 0.5 mm diameter orifice into the vacuum. When measurements are performed on the free DPA molecule, Ne or sometimes Ar is used as carrier gas, while pure Ar, Kr, and Xe are used for measurements on the respective van der Waals complexes. The laser-desorbed molecules are entrained in the jet and their internal energy is efficiently re-
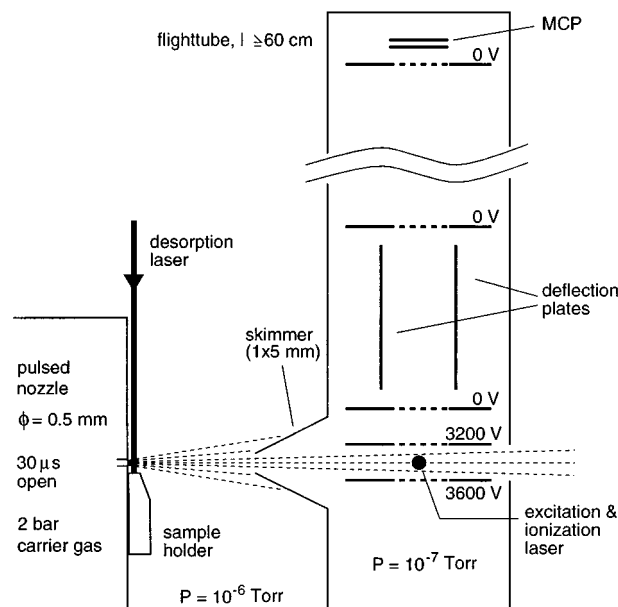

FIG. 1. Scheme of the laser desorption jet cooling mass spectrometer. DPA molecules are laser-desorbed out of a piece of charcoal that is positioned near the orifice of a pulsed valve. The molecular beam is skimmed upon entering the differentially pumped mass spectrometer. Molecules are photo-ionized and mass-selectively detected at the end of a Wiley–McLaren type linear TOF set-up.

duced by multiple collisions in the expansion region. Rovibrational temperatures comparable to temperatures obtained in ``conventional'' molecular beam seeding experiments are obtained in this way.[23] The piece of active carbon can contain a large quantity of DPA that is slowly released from the bulk to the surface of the matrix. DPA is desorbed from the top layers of the charcoal by the desorption laser pulse, and is replenished by migration from the bulk in between laser pulses. In this way a stable source of laser-desorbed jet-cooled DPA is obtained that lasts for several hours. The molecular beam is skimmed upon entering the differentially pumped Wiley–McLaren type linear time-of-flight (TOF) mass spectrometer.

The molecules in the beam interact with the incoming laser light at the crossing point of the mutually perpendicular molecular beam axis, laser beam axis, and TOF-tube axis, indicated by the small circle in Fig. 1. Ions produced in this region are extracted and accelerated into the field-free drift region by the electric fields present between the electrodes of the mass spectrometer. The ions are detected at the end of the TOF tube by a dual microchannelplate (MCP) detector. In most experiments, a 60 cm long TOF tube is used, yielding a mass resolution $M/\Delta M \approx 400$. This is sufficient for isotope resolved detection of the various DPA van der Waals complexes.

The signal from the MCP detector is fed into a 10 bit, 100 Megasamples/s digital oscilloscope (LeCroy 9430) that is connected to a PC via a GPIB interface. The data are further processed within the PC that also controls the wavelength scans of the excitation laser as well as the settings of
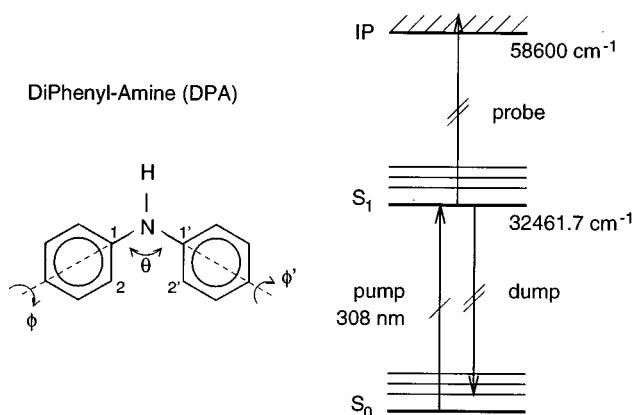
DiPhenyl-Amine (DPA)

FIG. 2. The molecule diphenylamine (DPA, 169 Da) is shown left, together with the definition of the torsional angles ϕ and ϕ' of the phenyl groups around the C-N bonds and the C-N-C bond angle θ. The two-color REMPI schemes that have been applied to the molecule, are indicated in the right part of the figure.

two four-channel digital delay/pulse-generators (Stanford Research Systems, DG535).

DPA is measured via a two-color $(1+1')$-resonance-enhanced multiphoton ionization (REMPI) scheme, as indicated in the right part of Fig. 2. The structure of the molecule is indicated in the left part of that figure, together with the definition of some geometrical parameters. For the measurement of the REMPI spectra via the S_1-state, laser excitation to this state is performed with a frequency-doubled, 0.15 cm^{-1} bandwidth pulse from a tunable dye-laser (Spectra-Physics, PDL-3) that is pumped by a frequency-doubled pulse from a Nd:YAG-laser (Spectra-Physics, GCR-150). Part of the same Nd:YAG-laser pulse is frequency-tripled and this 355 nm pulse is used for subsequent ionization from the S_1-state. The pathlengths of the two light pulses are matched to ensure simultaneous arrival of the counterpropagating pulses in the interaction region. An advantage of this particular two-color REMPI scheme is that three or more 355 nm photons are needed for non-resonant ionization of DPA, making this a very low probability process. Consequently, a high ionization laser fluence can be used leading to a high REMPI efficiency, while the excitation laser fluence can be kept low, thereby avoiding the occurrence of broadening mechanisms. The excitation laser is used with a fluence of ≈ 1 MW/cm^2 and the ionization laser with ≈ 20 MW/cm^2. The peak absorption cross section of DPA on the origin of the $S_1 \leftarrow S_0$ transition and for ionization from the S_1-state is $\sigma_{exc} = 1.1 \times 10^{-16}$ cm^2 and $\sigma_{si} \lesssim 5 \times 10^{-18}$ cm^2, respectively,[24] from which it is concluded that the laser excitation and ionization steps are still well away from saturation. The fundamental frequency of the excitation laser has been calibrated by the simultaneous measurement of I_2 absorption lines, that are tabulated to high accuracy.[27] The relative pulse energy of the excitation laser is recorded simultaneously with the ion signal, and the REMPI spectra presented in this paper are all corrected for variations in the excitation laser fluence over the scanning range.

In the ion-dip experiment[28,29] population is pumped to an energy level in the S_1-state of DPA with a resonant, 0.4 cm^{-1} bandwidth, pulse from a Nd:YAG pumped, frequency-doubled dye-laser (Spectra-Physics, GCR-11/PDL-2 combination) that is fixed in frequency. Ionization from this energy level is performed with the more intense Nd:YAG/dye-laser combination mentioned earlier (GCR-150/PDL-3). While scanning the ionization laser on the red side of the pump laser, it can become resonant with transitions back to vibrational levels in the electronic ground state S_0. Dips will appear in the two color ion signal whenever stimulated emission pumping (SEP) to these levels occurs.[30] The frequency difference between the preparation (pump) and ionization (dump) laser is then a direct measure of the vibrational frequency of the DPA molecule in the S_0-state. A disadvantage of the ion-dip technique is its inherent low signal to noise (S/N) ratio as one has to detect dips in a large ion background signal. In addition, only a limited fraction of the upper state population can be dumped back to the S_0-state.[30] To optimize the contrast, the fluence of the pump laser is kept a factor 15 to 20 lower than that of the dump laser.

The REMPI spectra of the vdW-complexes of DPA with the carrier gas atoms Ar, Kr, and Xe have been recorded under the same experimental conditions as those of the monomer measurements. The time-delay between desorption laser and REMPI lasers has of course been adapted to the speed of the employed carrier gas in the expansion.[26]

III. RESULTS AND ANALYSIS

A. REMPI spectroscopy via the S_1-state

Figure 3 shows the first 1000 cm^{-1} of the excitation spectrum to the S_1-state of DPA, measured via two-color $(1+1')$-REMPI with mass-selective ion detection. The spectrum has been measured by stepping the dye-laser in 0.25 cm^{-1} intervals, and averaging over 20 laser pulses at each wavelength. The electronic origin of the $S_1 \leftarrow S_0$ transition in DPA lies at (32461.7 ± 0.1) cm^{-1}. The full width at half maximum (FWHM) of the transition is determined by its rotational envelope, and amounts to (1.7 ± 0.1) cm^{-1} under the laser-desorption jet-cooling conditions in the experiments reported here. The bandwidth of the pulsed dye-lasers does not allow resolution of rotational structure. The lifetime of the S_1-state has been determined by scanning the time delay between excitation and ionization laser. Two color ionization signal is only observed when the two light pulses overlap in time. It is therefore concluded that the lifetime of the excited state has an upper limit of 5 ns. This short lifetime is due to rapid intersystem crossing (ICS) to triplet states.[24,25] In solution, a fluorescence lifetime of singlet excited DPA of 3 ns has been determined.[6]

The REMPI spectrum consists of many vibrational lines and the major part of the activity in the electronic spectrum is carried by two low-frequency vibrational modes that most likely involve the motion of the phenyl-rings as entities relative to the frame of the molecule. The most prominent vibrational mode has a frequency of (62.1 ± 0.3) cm^{-1}, while the second one has a frequency of (89.7 ± 0.3) cm^{-1} (see Sec.
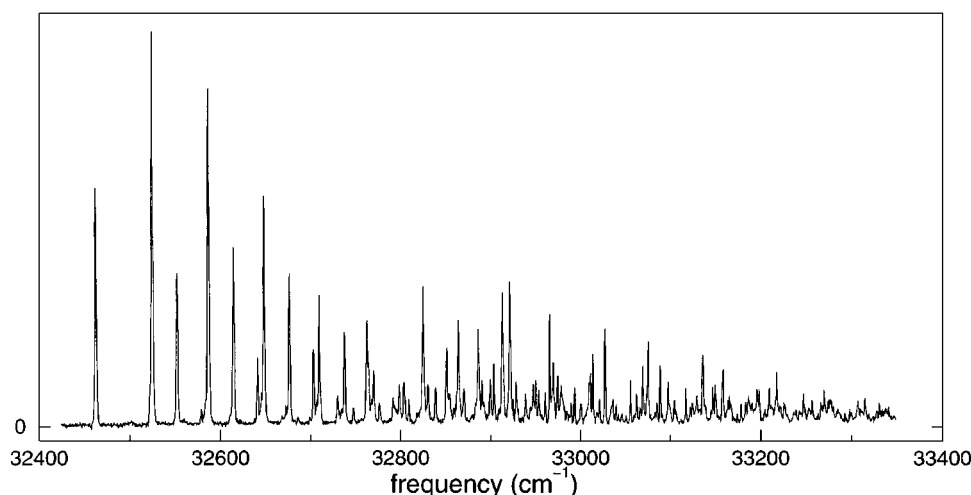
FIG. 3. Two-color $(1+1')$-REMPI spectrum of the $S_1 \leftarrow S_0$ transition in laser-desorbed jet-cooled DPA in the 309–305 nm range. The electronic origin of the transition lies at (32461.7 ± 0.1) cm^{-1}. Long Franck–Condon progressions in two low-frequency modes as well as their combination bands dominate the spectrum. The frequencies of these modes are 62.1 cm^{-1} and 89.7 cm^{-1}. These frequencies belong to the motion of the phenyl groups relative to the frame of the molecule.

V A for a description of these modes). These modes exhibit long Franck–Condon induced progressions, which is an indication for a large change in the equilibrium geometry of the molecule in the $S_1 \leftarrow S_0$ transition. From these progressions, it can be seen that the anharmonicity of these two modes is small. Furthermore, they combine with each other, yielding a characteristic pattern, also indicated in the upper trace of Fig. 5. This pattern is repeated in combination with nearly all other vibrational modes, and therefore the excitation spectrum rapidly becomes congested. Hardly any hot bands are observed, although some spectra show a weak hot band ≈ 35 cm^{-1} *above* the electronic origin (see also Sec. V A). A list of all lines observed in the excitation spectrum of DPA, with frequencies, intensities and assignment, is compiled in Table IV. The fundamental frequencies of the observed modes are listed in Table I. The observed modes are enumerated according to increasing frequency.

The excitation spectrum of DPA containing a ^{13}C-isotope is simultaneously measured by recording the ion signal on mass 170 Da. The electronic origin of the $S_1 \leftarrow S_0$ transition for this species lies at (32463.4 ± 0.2) cm^{-1}, corresponding to a blueshift of (1.7 ± 0.2) cm^{-1} relative to the DPA origin measured at 169 Da. The blueshift decreases with increasing frequency in the excitation spectrum due to the mass difference. The spectrum of the isotopically substituted DPA is otherwise identical to the spectrum of nonsubstituted DPA and has line intensities of 10% relative to that. Based on a 1.1% natural ^{13}C abundance this ratio should be 13.4%. The discrepancy can be explained by the larger linewidth for the transition of the isotopomer, being (2.8 ± 0.1) cm^{-1}. This is due to the slightly different line positions for the various ^{13}C^{12}C$_{11}$H$_{10}$NH isomers of DPA at 170 Da, as opposed to the more sharply defined line position for the one existing ^{169}DPA isomer.

To support the analysis and assignment of the vibrational lines in the excitation spectrum of DPA, the spectrum of the

deuterated species, i.e., DPA with the amine proton replaced by a D-atom, has been measured in the same setup by recording the ion signal on mass 170 Da. As the shift in vibrational frequency will depend on the degree of participation of the D-atom in the corresponding motion, it will be different for the various vibrational modes. Deuterated diphenylamine (D-DPA) is obtained by soaking a piece of charcoal filled with DPA in D$_2$O for some hours. The resulting fraction of D-DPA ranges from 65 to 80%. The contribution of the ^{13}C-isotopomer of ''normal'' DPA (H-DPA) to the signal on

TABLE I. Experimentally observed fundamental S_1-state vibrational frequencies for H-DPA (169 Da) and D-DPA (170 Da), compared to the calculated normal mode frequencies of these molecules in the S_1 and in the S_0-state. The frequencies are calculated from the 6-31G* and the 6-31G** basis set, respectively. The arguments for the correlation between experimental and calculated frequencies, between H-DPA and D-DPA frequencies, and between excited and ground state frequencies are discussed in the text. The frequencies are all given in wave numbers. The experimental values have an accuracy of 0.3 cm^{-1}.

|	H-DPA			D-DPA		
	S_1		S_0	S_1		S_0
Mode	Expt.	Calc. (symm)	Calc.	Expt.	Calc. (symm)	Calc.
ν_1	59.1	73.7 (B)	26.2	58.6	74.4 (B)	26.0
ν_2	62.1	53.9 (A)	104.4	62.1	53.8 (A)	104.1
ν_3	89.7	91.4 (A)	47.5	89.9	91.4 (A)	47.3
ν_4	⋯	222.0 (B)	227.1	198.2	217.0 (B)	205.0
ν_5	223.8	226.8 (A)	251.1	223.9	226.7 (A)	250.9
ν_6	300.4	325.7 (A)	315.5	300.2	325.6 (A)	260.3
ν_7	341.6	364.1 (B)	393.7	⋯	349.4 (B)	392.8
ν_8	441.9	429.7 (A)	544.3	442.5	429.5 (A)	542.5
ν_9	451.4(?)	447.4 (B)	563.6	⋯	421.9 (B)	562.8
ν_{10}	459.5(?)	467.6 (A)	461.4	⋯	457.9 (A)	461.4
ν_{11}		471.1 (B)	457.2	⋯	467.6 (B)	456.9
ν_{12}	552.0	573.2 (B)	622.7	549.1	551.7 (B)	613.3
⋮	⋮	⋮	⋮	⋮	⋮	⋮
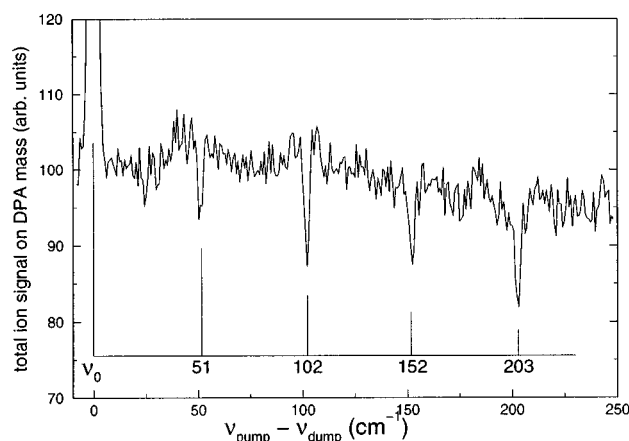
FIG. 4. Double resonance ion-dip spectrum of DPA, obtained by pumping the vibrationless level in the S_1-state. Resonances with transitions back to levels in the electronic ground state appear as dips in the two-laser ion signal. The ion signal is plotted as a function of the frequency difference between the lasers. A vibrational progression with a frequency spacing of 51 cm^{-1} is indicated.

mass 170 Da is in this case limited to ≈5% and is spectrally sufficiently separated to allow unambiguous assignment.

The general appearance of the excitation spectrum of D-DPA is very similar to that of H-DPA. Differences between the two spectra are only visible upon close inspection. One interesting difference is a weak progression starting at (198.2 ± 0.3) cm^{-1} that has apparently no counterpart in the H-DPA spectrum. Its cause will be discussed later. The electronic origin of the $S_1 \leftarrow S_0$ transition for deuterated diphenylamine lies at (32457.3 ± 0.1) cm^{-1}, which corresponds to a red shift of (4.4 ± 0.1) cm^{-1} relative to the DPA origin, and has a linewidth of (1.7 ± 0.1) cm^{-1} (FWHM). All lines observed in the D-DPA spectrum are listed with frequency, intensity and assignment in Table V, and the fundamental frequencies assigned to normal modes are listed together with those of H-DPA in Table I.

B. Double resonance ion-dip spectroscopy on the S_0-state

A characteristic ion-dip spectrum of DPA is presented in Fig. 4. In this measurement the pump laser has been used to prepare the vibrationless level in the S_1-state of DPA. In the figure the ion yield on mass 169 Da is shown as a function of the frequency difference between pump and dump laser. The position of ion dips is, therefore, directly related to vibrational frequencies in the S_0-state of DPA.

Four dips, equally spaced in frequency, can be observed in the spectrum. They correspond to a decrease of the two-color ion signal with ≈14%. The dips form a Franck–Condon progression of a vibrational mode in the electronic ground state with a frequency of (51.2 ± 0.5) cm^{-1}. Ion-dip spectra have been taken from several vibrational levels in the S_1-state. In all spectra, only dips belonging to this same Franck–Condon progression have been observed. Apparently, these are the strongest lines in the $S_1 \rightarrow S_0$ transition.

From this observation, and from the value of the frequency, it is concluded that this mode has similar characteristics to that of the 62.1 cm^{-1} mode in the S_1-state. Surprisingly, a mode corresponding to the 89.7 cm^{-1} mode in the S_1-state is not observed. An explanation for the apparent absence of this mode might be that its S_0-frequency is nearly equal to 2×51 cm^{-1}, as is suggested by the calculations (see Sec. IV B). In that case the mode will be hidden under the 51 cm^{-1} progression.

C. REMPI on the van der Waals complexes of DPA with Ar, Kr, and Xe

The REMPI spectra of the van der Waals complexes of DPA with the carrier gas atoms Ar, Kr, and Xe are shown in Fig. 5 together with the first 300 cm^{-1} of the DPA monomer spectrum. These spectra provide additional information on the monomer as symmetry is broken in the excited state of the complex, leading to the appearance of formerly (partly) forbidden lines. Furthermore, the spectra of the vdW-complexes with DPA contain information on the influence of the vdW-bonded atom on the motion of the phenyl rings relative to the frame of the molecule.

The spectra are measured by recording the ion signal on the mass of the respective complexes. For DPA-Ar, spectral hole burning experiments have been performed to confirm that the observed spectral structure is due to a single vdW-species. Due to the various Kr and Xe isotopes, the signal on the DPA-Kr and DPA-Xe complexes is distributed over several masses. The spectra of the vdW-complexes with the various isotopes of Kr or Xe are found to be identical within the spectral resolution. In the figure, therefore, the sum of the spectra of the various isotopomers of DPA-Kr and DPA-Xe are shown. The DPA-Ne complex could not be observed. Apparently the binding energy of this complex is so low that the expansion conditions in the laser desorption molecular beam source do not allow its formation. The absence of DPA-Ne complexes can be used to advantage, as it makes Ne an ideal carrier gas for the measurement of ''clean and pure'' DPA-spectra.

From a comparison of the spectra in Fig. 5 a few observations can be made. The general shape of the spectra of the vdW-complexes, i.e., the characteristic pattern of Franck–Condon progressions and combination bands of low-frequency vibrational modes, is similar to that of the monomer. However, the spectra of the vdW-complexes become congested very rapidly. After a few hundred wave numbers, individual lines can no longer be identified.

The $S_1 \leftarrow S_0$ transitions in the vdW-complexes show a red shift with respect to the transition in the monomer. This shift is (25.0 ± 0.3) cm^{-1} for DPA-Ar, (42.6 ± 0.3) cm^{-1} for DPA-Kr, and (66.2 ± 0.3) cm^{-1} for DPA-Xe. Both the redshift of the electronic origin upon complexing, as well as its observed increase with increasing polarizability of the rare gas atom, are commonly observed in vdW-complexes where the rare gas atom is positioned on top of an aromatic ring.[31]

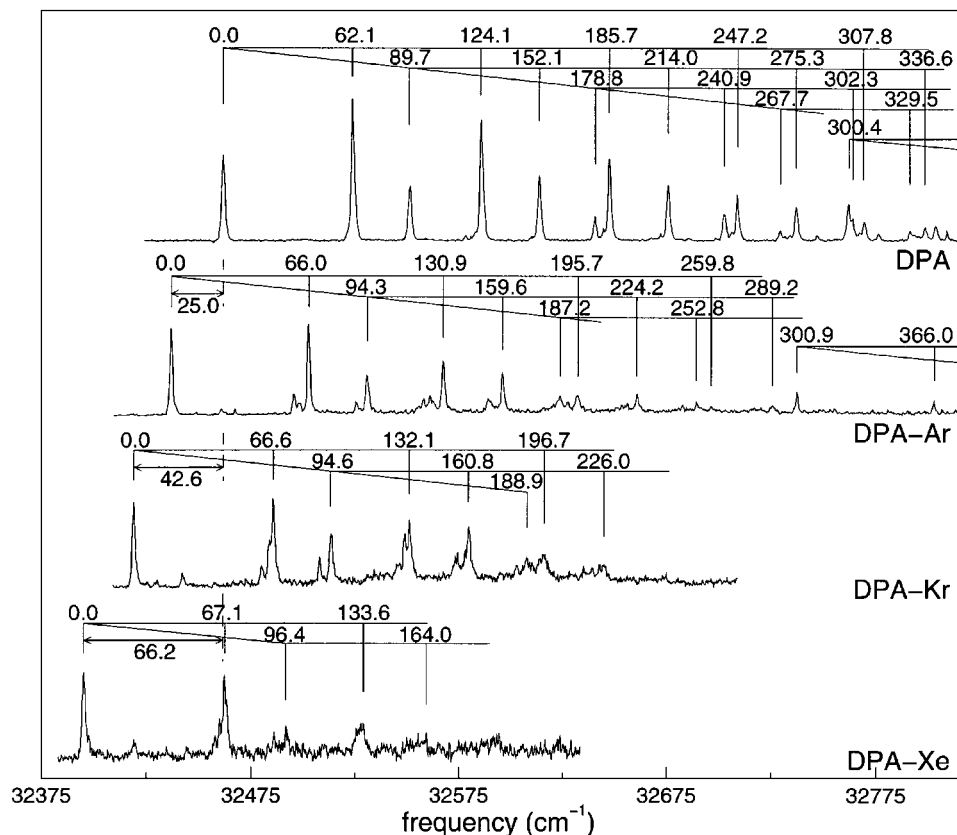The complex spectra show additional structure around

FIG. 5. From top to bottom are shown the mass-selected two-color $(1+1')$-REMPI spectra of DPA and of the van der Waals complexes DPA-Ar, DPA-Kr, and DPA-Xe. The spectra are scaled to have equally high electronic origins and are plotted on an absolute frequency scale. The redshift of the transition in the vdW-complex relative to that in the monomer is given by the distance from the dashed line that indicates the position of the electronic origin of DPA. The Franck–Condon progressions in the DPA excitation spectrum, indicated above the spectrum, are also present in the spectra of the vdW-complexes.

the mode that corresponds to the 62.1 cm^{-1} mode in the monomer. Two extra lines are observed that cannot both be attributed to van der Waals modes. One of the extra lines is due to an intramolecular mode that is hidden in the monomer spectrum. The clear appearance of this line in the spectra of the vdW-complexes is one of the strongest indications for the existence of this particular mode, as discussed in Section V A. The additional lines at low frequencies are attributed to van der Waals modes. The three vdW-modes may or may not combine with intra-molecular vibrational modes.

There is a rather large increase in the three lowest intra-molecular excited state frequencies of DPA upon complex-ing. This increase differs for the various modes, ranging from ≈4% for the 59.1 cm^{-1} mode (ν_1) to ≈7% for the 62.1 cm^{-1} mode (ν_2). Furthermore, the increase is getting larger with increasing mass of the rare gas atom. No frequency change is observed for the 300.4 cm^{-1} mode (ν_6). Table II lists the frequencies of the fundamental intramolecular and van der Waals modes, as well as the observed electronic origin of the vdW-complexes. The assignment of the vdW-modes is tentative, as it cannot be excluded that overtones and/or combination bands appear in the electronic spectrum rather than the fundamental modes. Lists of all observed lines in the spectra of the DPA-Ar, DPA-Kr, and DPA-Xe

vdW-complexes are given in Tables VI, VII, and VIII, re-spectively.

IV. AB INITIO CALCULATIONS

A. Computational methods

The geometry and frequencies of DPA are calculated both in the electronic ground state and in the first singlet

TABLE II. Comparison of excited state properties of DPA and the vdW-complexes DPA-Ar, DPA-Kr, and DPA-Xe. Intramolecular vibrational modes are denoted with ν_i, while ω_j denotes a van der Waals mode. Frequencies are all given in wave numbers with an accuracy of 0.3 cm^{-1}.

	DPA	DPA-Ar	DPA-Kr	DPA-Xe
Electronic origin	32461.7	32436.7	32419.1	32395.5
intramolecular vibrational frequencies				
ν_1	59.1	61.5	61.2	62.3
ν_2	62.1	66.0	66.6	67.1
ν_3	89.7	94.3	94.6	96.4
ν_4	···	···	···	···
ν_5	223.8	···	···	···
ν_6	300.4	300.9	···	···
van der Waals frequencies				
ω_1		24.0	23.4	24.0
ω_2		30.6	···	···
ω_3		59.0	65.0	64.7

TABLE III. Parameter values resulting from the *ab initio* geometry optimization. The definition of the parameters can be found in Fig. 2. β is the ''inversion angle'' between the N-H bond and the C1-N-C1$'$ plane. The angles are in degrees, and the bond lengths in Å. For a comparison also the values resulting from calculations with the semi-empirical CNDO/2 method by Pankratov *et al.* (Ref. 12) are given.

Method	State	ϕ	ϕ'	β	θ	C1-N-H	C1$'$-N-H	C1-N	C1$'$-N	N-H
CIS (6-31G*)	S_1	27.0	27.0	0.0	126.7	116.7	116.7	1.369	1.369	1.000
HF (6-31G**)	S_0	14.7	44.5	20.8	126.9	114.5	114.9	1.401	1.399	0.993
CNDO/2	S_0	13.8	34.1	26.7	124.1	116.4	113.1	⋯	⋯	⋯

excited state using the program GAUSSIAN 94.[32] For the ground state, the geometry has been optimized at the Hartree–Fock (HF) level using the 6-31G(d,p) basis set. No symmetry constraints are applied. The resulting optimized geometry has no symmetry and a subsequent harmonic frequency calculation showed no imaginary frequencies. The two phenyl groups are not equivalent, one having a torsional angle $\phi = 14.7°$ with respect to the C-N-C plane while the other ring has a torsional angle $\phi' = 44.5°$. The hydrogen atom bound to the nitrogen is tilted out of the C-N-C plane. The resulting ''inversion angle'' of the N-H bond with respect to the C-N-C plane is found to be $\beta = 20.8°$. For a definition of the geometrical parameters see Fig. 2. It seems that, due to the tilt of the phenyl rings, the lone pair on the nitrogen cannot efficiently take part in the conjugation of the phenyl rings and, therefore, a non-planar configuration local to the N-atom is preferred. The inversion angle of DPA can be compared to the same angles for ammonia (NH$_3$), which has $\beta = 80°$,[33] aniline with $\beta \approx 37°$,[34] and triphenylamine (TPA) where $\beta \approx 0°$.[35] This comparison reveals an obvious trend in the configuration around N that changes from a pyramidal to a planar geometry with the consecutive addition of phenyl-groups. Because of its smoothness, we believe that this trend results from an increasing delocalization of the N lone pair orbital, along with a gradual transition from a sp^3 to a sp^2 state of hybridization of the N-nucleus. Some geometrical parameters are given in Table III and the twelve lowest frequencies are listed in Table I.

The S_1-state is calculated by a configuration interaction (CI) calculation that includes all single excitations (CIS). Due to computational restrictions, the additional p-orbitals on the hydrogen atoms are left out and the 6-31G(d) basis set is used. The electronic term energy is calculated to be 5.46 eV. Corrected for the difference in zero point energy, the excitation energy results in 5.33 eV. The experimental value for the origin of the electronic transition is 4.02 eV. The subsequent analytical frequency calculation at the CIS level showed no imaginary frequencies. The two phenyl rings are equivalent, each having a torsional angle $\phi = \phi' = 27.0°$ with respect to the C-N-C plane. The sum of the torsional angles thus decreases 5.2° in going from the S_0 to the S_1-state. The hydrogen atom bound to the nitrogen is found to lie in the C-N-C plane. The S_1-state is thus found to have C_2 symmetry, in contrast to the C_1 symmetry of the ground state.

The dominant excitation, with a CI coefficient of 0.69, corresponds to a direct HOMO-LUMO excitation in DPA.

The two orbitals have, in the point group of the excited state, A and B symmetry, respectively, resulting in a ^1B S_1-state. This excitation occurs from a strongly localized orbital on the nitrogen atom (lone pair) to a delocalized orbital on the two phenyl rings with π^* character ($\pi^* \leftarrow n$ transition). This is consistent with the findings of Huber and co-workers who concluded that the lowest transitions in DPA have substantial charge-transfer character.[3–6] The planarity around the nitrogen atom in the S_1-state comes, therefore, as no surprise since the local electronic configuration is similar to that of the (planar) NH$_3^+$ ion. The other important excitations for that state occur on the phenyl rings and correspond to $\pi \rightarrow \pi^*$ excitations. Geometrical parameters are shown in Table III and vibrational frequencies in Table I.

There are not many experimental or theoretical studies that allow a comparison of the results of the calculations. All experimental data on torsional and bond angles come from studies in the condensed state. Here, we only want to mention the good agreement between the calculated Cl-N-Cl$'$ bond angle $\theta = 126.9°$ in the ground state and the value $\theta = 126°$ obtained from X-ray diffraction measurements.[16] Ito *et al.* have thus far been the only ones to perform *ab initio* MO calculations, but they restricted the calculations to fixed geometries and their results are, therefore, not comparable to ours. We can, however, compare our results to those of Pankratov and coworkers,[12] who optimized the geometry of DPA with semi-empirical methods. Their geometry optimization of DPA in the electronic ground state with the CNDO/2 method already predicted a pyramidal configuration around N, non-equal torsional angles, and bond angles that agree rather well with the present calculations. Some of their CNDO/2 results are included in Table III.

B. Vibrational modes

The DPA molecule, (C$_6$H$_5$)$_2$NH, has 24 atoms and therefore 66 vibrational degrees of freedom. In order to understand the vibrational modes of DPA, it is illustrative to decompose them into local modes. Assuming the phenyl rings to be internally rigid, 12 degrees of freedom are left. These 12 modes result from 6 ''ammonialike'' modes and 3 modes of each rigid phenyl ring with respect to the rest of the molecule. Two of these 3 modes are bending modes of the phenyl plane with respect to the phenyl-N bond and one is the rotation of the phenyl ring around the phenyl-N bond. A total of 54 modes are left over for motion within the phenyl rings.

TABLE IV. Experimentally observed lines in the excitation spectrum of the first electronically excited singlet state of diphenylamine (DPA, mass 169 Da). The frequencies are given in wave numbers relative to the electronic origin of DPA at (32461.7 ± 0.1) cm^{-1}. The intensities are relative to the intensity of the electronic origin, which is set to 100. s denotes a shoulder. In the assignment a $+$ denotes a combination band, and the mode that is expected to have the largest contribution to the line is mentioned first.

Frequency	Intensity	Mode
0.0	100	origin
59.1	(s)	ν_1
62.1	166	ν_2
89.7	64	ν_3
116.6	7	$2\nu_1$
121.3	11 (s)	$\nu_1+\nu_2$
124.1	142	$2\nu_2$
148.1	5 (s)	$\nu_1+\nu_3$
152.1	75	$\nu_3+\nu_2$
178.8	28	$2\nu_3$, $2\nu_1+\nu_2$
183.0	15 (s)	$\nu_1+2\nu_2$
185.7	96	$3\nu_2$
205.7	5	$2\nu_1+\nu_3$, ν_4 ?
210.3	8 (s)	$\nu_1+\nu_3+\nu_2$
214.0	64	$\nu_3+2\nu_2$
223.8	4	ν_5
237.2	4	$\nu_1+2\nu_3$
240.9	32	$2\nu_3+\nu_2$, $2\nu_1+2\nu_2$
244.8	11 (s)	$\nu_1+3\nu_2$
247.2	55	$4\nu_2$
267.7	13	$3\nu_3$
270.0	6 (s)	$2\nu_1+\nu_3+\nu_2$
272.4	7 (s)	$\nu_1+\nu_3+2\nu_2$
275.3	39	$\nu_3+3\nu_2$
285.5	8	$\nu_5+\nu_2$
294.1	3	$2\nu_1+2\nu_3$
300.4	44	ν_6, $\nu_1+2\nu_3+\nu_2$
302.3	27 (s)	$2\nu_3+2\nu_2$, $2\nu_1+3\nu_2$
305.5	11 (s)	$\nu_1+4\nu_2$
307.8	23	$5\nu_2$
314.4	9	$\nu_5+\nu_3$
325.6	3	$\nu_1+3\nu_3$
329.5	12	$3\nu_3+\nu_2$
331.1	8 (s)	$2\nu_1+\nu_3+2\nu_2$
333.5	7	$\nu_1+\nu_3+3\nu_2$
336.6	17	$\nu_3+4\nu_2$
341.6	18	ν_7
347.2	11	$\nu_5+2\nu_2$
356.0	6	$4\nu_3$
359.5	7 (s)	$\nu_6+\nu_1$, $\nu_1+2\nu_3+2\nu_2$
362.8	58	$\nu_6+\nu_2$, $2\nu_3+3\nu_2$, $2\nu_1+4\nu_2$
366.5	8 (s)	$\nu_1+5\nu_2$
368.4	18	$6\nu_2$
376.7	16	$\nu_5+\nu_3+\nu_2$
379.6	4 (s)	$\nu_4+3\nu_2$?
389.3	33	$\nu_6+\nu_3$, $\nu_1+3\nu_3+\nu_2$
392.4	14	$3\nu_3+2\nu_2$, $2\nu_1+\nu_3+3\nu_2$
394.8	7 (s)	$\nu_1+\nu_3+4\nu_2$
397.5	8	$\nu_3+5\nu_2$
400.0	12 (s)	?
402.3	44	$\nu_7+\nu_2$, $\nu_1+2\nu_3$?
405.1	9 (s)	?
408.4	16	$\nu_5+3\nu_2$
416.9	4	$\nu_6+2\nu_1$
418.2	5	$4\nu_3+\nu_2$
421.6	10 (s)	$\nu_6+\nu_1+\nu_2$, $\nu_1+2\nu_3+3\nu_2$
424.6	41	$\nu_6+2\nu_2$, $2\nu_3+4\nu_2$, $2\nu_1+5\nu_2$, $\nu_1+6\nu_2$
428.8	19	$7\nu_2$
430.9	10 (s)	$\nu_7+\nu_3$

TABLE IV. (*Continued.*)

Frequency	Intensity	Mode
434.1	6	?
437.9	20	$\nu_5+\nu_3+2\nu_2$
441.9	26	ν_8
447.6	7	$\nu_6+\nu_1+\nu_3$
451.4	56	ν_9, $\nu_6+\nu_3+\nu_2$, $\nu_1+3\nu_3+2\nu_2$, $3\nu_3+3\nu_2$, $2\nu_1+\nu_3+4\nu_2$
455.1	5	$\nu_1+\nu_3+5\nu_2$
459.5	60	ν_{10} ?
463.1	11	?
466.8	19	$\nu_7+2\nu_2$
468.8	(s)	$\nu_5+4\nu_2$
477.0		$\nu_6+2\nu_3$
479.9	(s)	$4\nu_3+2\nu_2$
482.5		$\nu_6+\nu_1+2\nu_2$, $\nu_1+2\nu_3+4\nu_2$
485.5		$\nu_6+3\nu_2$, $2\nu_3+5\nu_2$
488.7		$8\nu_2$, ?
492.1	15	$\nu_7+\nu_3+\nu_2$
499.1		$\nu_5+\nu_3+3\nu_2$
503.9	47	$\nu_8+\nu_2$
512.7	21	$\nu_6+\nu_3+2\nu_2$, $\nu_1+3\nu_3+3\nu_2$, $3\nu_3+4\nu_2$
516.7		?
528.1	9	$\nu_7+3\nu_2$
531.9	16	$\nu_8+\nu_3$, $\nu_5+5\nu_2$
539.0		$\nu_6+2\nu_3+\nu_2$
542.0	(s)	$4\nu_3+3\nu_2$
545.5	(s)	$\nu_6+\nu_1+3\nu_2$, $\nu_1+2\nu_3+5\nu_2$
547.7	(s)	$\nu_6+4\nu_2$, $2\nu_3+6\nu_2$
552.0	30	ν_{12}
556.7	6	$\nu_7+\nu_3+2\nu_2$
561.6	(s)	$\nu_5+\nu_3+4\nu_2$
565.6	41	$\nu_8+2\nu_2$
574.0		$\nu_6+\nu_3+3\nu_2$, $\nu_1+3\nu_3+4\nu_2$, $3\nu_3+5\nu_2$
589.0	5	$\nu_7+4\nu_2$
593.8	19	$\nu_8+\nu_3+\nu_2$
600.4		$\nu_6+2\nu_3+2\nu_2$, $2\nu_6$, ?
604.8		$\nu_6+\nu_1+4\nu_2$, $\nu_1+2\nu_3+6\nu_2$
607.4		$\nu_6+5\nu_2$, ?
613.4	35	$\nu_{12}+\nu_2$
616.3	5	$\nu_7+\nu_3+3\nu_2$
621.1	6	$\nu_8+2\nu_3$
626.9	25	$\nu_8+3\nu_2$
637.8	(s)	$\nu_6+\nu_3+4\nu_2$, $3\nu_3+6\nu_2$
642.7	11	$\nu_{12}+\nu_3$, $\nu_6+\nu_7$?
644.5	6 (s)	$\nu_6+2\nu_3+2\nu_2$
650.2	3	$\nu_7+5\nu_2$
655.3	16	$\nu_8+\nu_3+2\nu_2$
669.8		$\nu_6+6\nu_2$
673.8	30	$\nu_{12}+2\nu_2$
683.1	7	$\nu_8+2\nu_3+\nu_2$, $2\nu_7$?
687.7	17	$\nu_8+4\nu_2$
703.3	13	$\nu_{12}+\nu_3+\nu_2$
716.4	10	$\nu_8+\nu_3+3\nu_2$
734.0	16	$\nu_{12}+3\nu_2$
764.1	9	$\nu_{12}+\nu_3+2\nu_2$
794.7	11	$\nu_{12}+4\nu_2$
823.1	8	$\nu_{12}+\nu_3+3\nu_2$

The latter modes are expected to have frequencies higher than 400 cm^{-1} and are, therefore, only of limited interest for this study.

The calculated modes of DPA in its ^{1}B S_1-state have been visualized and categorized according to the local mode picture above. For the three lowest frequency vibrations, the

TABLE V. Experimentally observed lines in the excitation spectrum of the first electronically excited singlet state of deuterated diphenylamine $(C_6H_5)_2ND$ (D-DPA, mass 170 Da). The frequencies are given in wave numbers relative to the electronic origin of D-DPA at (32457.3 ± 0.1) cm^{-1}, which is (4.4 ± 0.1) cm^{-1} redshifted from the origin of DPA. The intensities are relative to the intensity of the electronic origin, which is set to 100. s denotes a shoulder. In the assignment a + denotes a combination band, and the mode that is expected to have the largest contribution to the line is mentioned first.

Frequency	Intensity	Mode
0.0	100	origin
58.6	12 (s)	ν_1
62.1	178	ν_2
89.9	63	ν_3
116.2	13	$2\nu_1$
121.3	19 (s)	$\nu_1+\nu_2$
123.7	171	$2\nu_2$
148.5	7 (s)	$\nu_1+\nu_3$
151.9	86	$\nu_3+\nu_2$
174.2	5	$3\nu_1$?
178.3	27 (s)	$2\nu_1+\nu_2$
178.7	28	$2\nu_3$
182.2	20 (s)	$\nu_1+2\nu_2$
185.0	130	$3\nu_2$
198.2	7	ν_4
205.2	8	$2\nu_1+\nu_3$
210.4	12 (s)	$\nu_1+\nu_3+\nu_2$
213.6	73	$\nu_3+2\nu_2$
223.9	8	ν_5
231.1	5	$4\nu_1$?
236.3	7	$\nu_1+2\nu_3, 3\nu_1+\nu_2$
239.8	21 (s)	$2\nu_1+2\nu_2$
240.9	33	$2\nu_3+\nu_2$
243.5	22	$\nu_1+3\nu_2$
246.0	78	$4\nu_2$
260.2	10	$\nu_4+\nu_2$
267.2	12 (s)	$2\nu_1+\nu_3+\nu_2$
267.8	13	$3\nu_3$
271.6	11 (s)	$\nu_1+\nu_3+2\nu_2$
274.6	49	$\nu_3+3\nu_2$
285.3	15	$\nu_5+\nu_2$
287.6	10	$\nu_4+\nu_3$
294.1	3	$2\nu_1+2\nu_3$
297.6	9 (s)	$\nu_1+2\nu_3+\nu_2, 3\nu_1+2\nu_2$
300.2	51	$\nu_6, 2\nu_1+3\nu_2$
302.3	28	$2\nu_3+2\nu_2$
303.8	22 (s)	$\nu_1+4\nu_2$
306.3	40	$5\nu_2$
314.5	14	$\nu_5+\nu_3$
321.0	16	$\nu_4+2\nu_2$
328.3	11 (s)	$2\nu_1+\nu_3+2\nu_2$
329.8	13	$3\nu_3+\nu_2$
332.8	11 (s)	$\nu_1+\nu_3+3\nu_2$
335.3	28	$\nu_3+4\nu_2$
346.6	30	$\nu_5+2\nu_2$, ?
349.3	18	$\nu_4+\nu_3+\nu_2$
358.6	11 (s)	$\nu_6+\nu_1, \nu_1+2\nu_3+2\nu_2, 3\nu_1+3\nu_2$
362.4	80	$\nu_6+\nu_2, 2\nu_1+4\nu_2$
363.5	(s)	$2\nu_3+3\nu_2, \nu_1+5\nu_2$
366.7	18	$6\nu_2$
376.5	27	$\nu_5+\nu_3+\nu_2$, ?
381.8	21	$\nu_4+3\nu_2$, ?
389.3	38	$\nu_6+\nu_3, 2\nu_1+\nu_3+3\nu_2, 3\nu_3+2\nu_2$
393.7	12	$\nu_1+\nu_3+4\nu_2$
397.0	22	$\nu_3+5\nu_2$, ?
406.9	30	$\nu_5+3\nu_2$, ?
410.4	20	$\nu_4+\nu_3+2\nu_2$, ?

TABLE V. (Continued.)

Frequency	Intensity	Mode
420.8	15	$\nu_6+\nu_1+\nu_2, 2\nu_1+5\nu_2$
424.0	63	$\nu_6+2\nu_2, 2\nu_3+4\nu_2, 7\nu_2$
437.6	35	$\nu_5+\nu_3+2\nu_2$, ?
442.5	35	ν_8
444.0	21 (s)	$\nu_4+4\nu_2$
450.9	49	$\nu_6+\nu_3+\nu_2, 3\nu_3+3\nu_2$
473.5	14	$\nu_4+\nu_3+3\nu_2$, ?
477.4	22	$\nu_6+2\nu_3, \nu_6+2\nu_1+\nu_2$
481.8	13 (s)	$\nu_6+\nu_1+2\nu_2$
495.1	34	$\nu_6+3\nu_2, 2\nu_3+5\nu_2$
504.2	63	$\nu_8+\nu_2$
512.1	37	$\nu_6+\nu_3+2\nu_2$
532.7	19	$\nu_8+\nu_3$
538.8	20	$\nu_6+2\nu_3+\nu_2, \nu_6+2\nu_1+2\nu_2$
545.9	15	$\nu_6+4\nu_2$
549.1	63	ν_{12}
565.1	47	$\nu_8+2\nu_2$
572.7	14	$\nu_6+\nu_3+3\nu_2$
594.2	24	$\nu_8+\nu_3+\nu_2$
600.1	22	$2\nu_6$?
605.0	13	$\nu_6+5\nu_2$
610.5	90	$\nu_{12}+\nu_2$
626.9	28	$\nu_8+3\nu_2$
634.0	11	$\nu_6+\nu_3+4\nu_2$
638.1	17	$\nu_{12}+\nu_3$
655.0	15	$\nu_8+\nu_3+2\nu_2$
671.2	74	$\nu_{12}+2\nu_2$
687.7	16	$\nu_8+4\nu_2$
698.8	18	$\nu_{12}+\nu_3+\nu_2$
716.6	13	$\nu_8+\nu_3+3\nu_2$
731.4	51	$\nu_{12}+3\nu_2$
743.4	27	$\nu_8+\nu_6$
759.0	12	$\nu_{12}+\nu_3+2\nu_2$
789.4	24	$\nu_{12}+4\nu_2$
804.5	25	$\nu_8+\nu_6+\nu_2$
818.3	13	$\nu_{12}+\nu_3+3\nu_2$
832.1	10	$\nu_8+\nu_6+\nu_3$
849.2	21	$\nu_{12}+5\nu_2, \nu_{12}+\nu_6$, ?

most important local mode contributions are: the in-phase wagging of the phenyl-rings in the C-N-C plane (53.9 cm^{-1}, A-symm.), the ''through-plane'' N-motion which is the equivalent of the ''umbrella motion'' in ammonia (73.7 cm^{-1}, B-symm.), and the in-phase torsion of the phenyl-rings around the C-N bonds (91.4 cm^{-1}, A-symm.). Four additional normal modes, that do not involve motion within the phenyl rings, are present below 400 cm^{-1} ($\nu_4-\nu_7$). The next four modes ($\nu_8-\nu_{11}$) are out-of-plane ring deformations, followed by four in-plane ring deformations ($\nu_{12}-\nu_{15}$). Higher frequencies are not analysed in this study.

The same visual inspection is done for the electronic ground state vibrational modes. It is instructive to correlate the ground and excited state modes and frequencies. This correlation is done on the basis of the local modes involved as well as on the approximate symmetry of the modes, and is shown in Table I. It should be noted, however, that this correlation is determined by eye and therefore only tentative.

TABLE VI. Experimentally observed lines in the excitation spectrum of the first electronically excited singlet state of the DPA-Ar van der Waals complex (mass 209 Da). The frequencies are given in wave numbers relative to the electronic origin of DPA-Ar at (32436.7 ± 0.3) cm^{-1}, which is (25.0 ± 0.3) cm^{-1} redshifted from the origin of DPA. The intensities are relative to the intensity of the electronic origin, which is set to 100. s denotes a shoulder. In the assignment intramolecular vibrational modes are denoted with ν_i, while ω_j denotes a van der Waals mode. A + denotes a combination band, and the mode that is expected to have the largest contribution to the line is mentioned first.

Frequency	Intensity	Mode
0.0	100	origin
12.1	4	?
24.1	7	ω_1
30.6	7	ω_2
59.0	25	ω_3
61.5	14	ν_1
66.0	103	ν_2
89.1	16	$\nu_2+\omega_1$, $\omega_2+\omega_3$
90.8	8 (s)	?
94.3	46	ν_3
119.1	11	$2\omega_3$, $\nu_3+\omega_1$, $\nu_2+\omega_1+\omega_2$, ?
121.5	19	?
124.5	22	$\omega_3+\nu_2$
125.8	17	$\nu_1+\nu_2$
130.9	62	$2\nu_2$
152.6	19	$\nu_3+\omega_3$
153.7	17 (s)	$\nu_1+\nu_3$, $2\nu_2+\omega_1$
159.6	48	$\nu_3+\nu_2$, $2\nu_2+\omega_2$
183.9	13	$\nu_3+\nu_2+\omega_1$
187.2	23	$2\nu_3$, $2\nu_2+\omega_3$, $\nu_3+\nu_2+\omega_2$, ?
191.1	16	$\nu_1+2\nu_2$
195.7	23	$3\nu_2$
214.4	10	$\nu_3+2\omega_3$, ?
216.9	12	$\nu_3+\nu_2+\omega_3$?
219.6	14	$\nu_1+\nu_3+\nu_2$, ?
224.2	25	$\nu_3+2\nu_2$
246.0	12	$2\nu_3+\omega_3$
252.8	16	$2\nu_3+\nu_2$
259.8	11	$4\nu_2$
280.1	9	$3\nu_3$
283.6	9	$\nu_3+2\nu_2+\omega_3$, ?
289.2	12	$\nu_3+3\nu_2$
300.9	27	ν_6
304.5	7	$2\nu_3+2\omega_3$?
311.7	8	$2\nu_3+\nu_2+\omega_3$
316.7	8	$2\nu_3+2\nu_2$
318.9	9	?
324.4	5	$5\nu_2$
337.0	7	?
344.1	7	$3\nu_3+\nu_2$
358.9	6	$\nu_6+\omega_3$
366.0	16	$\nu_6+\nu_2$
370.1	6	?
376.3	7	?
383.5	5	$2\nu_3+3\nu_2$
393.7	11	$\nu_6+\nu_3$
430.7	9	$\nu_6+2\nu_2$

TABLE VII. Experimentally observed lines in the excitation spectrum of the first electronically excited singlet state of the DPA-Kr van der Waals complex, recorded on mass 253 and 255 Da. The frequencies are given in wave numbers relative to the electronic origin of DPA-Kr at (32419.1 ± 0.3) cm^{-1}, which is (42.6 ± 0.3) cm^{-1} redshifted from the origin of DPA. The intensities are relative to the intensity of the strongest line, ν_2, which is set to 100. s denotes a shoulder. In the assignment intramolecular vibrational modes are denoted with ν_i, while ω_j denotes a van der Waals mode. A + denotes a combination band, and the mode that is expected to have the largest contribution to the line is mentioned first.

Frequency	Intensity	Mode
0.0	96	origin
23.4	18	ω_1
61.2	25	ν_1
65.0	54 (s)	ω_3
66.6	100	ν_2
89.0	35	$\nu_2+\omega_1$
94.6	60	ν_3
118.1	17	$\nu_3+\omega_1$
126.1	27	$\nu_1+\omega_3$
127.5	28	$\nu_1+\nu_2$
129.9	61	$\nu_2+\omega_3$
132.1	76	$2\nu_2$
154.3	35	$2\nu_2+\omega_1$
155.5	40	$\nu_1+\nu_3$
159.1	42 (s)	$\nu_3+\omega_3$
160.8	69	$\nu_3+\nu_2$
183.9	25	$\nu_3+\nu_2+\omega_1$
188.9	34	$2\nu_3$
190.1	29	$\nu_1+\nu_2+\omega_3$
191.3	29	$\nu_1+2\nu_2$
194.9	33	$2\nu_2+\omega_3$
196.7	38	$3\nu_2$
216.1	24	?
220.3	23	$\nu_1+\nu_3+\nu_2$
223.7	27	$\nu_3+\nu_2+\omega_3$
226.0	27	$\nu_3+2\nu_2$

V. DISCUSSION

A. Diphenylamine: structure and low-frequency vibrations

The abundance of fundamental modes contributing to the REMPI spectrum is in accord with an expected low sym-metry of the DPA molecule. This is confirmed by the calculations that predict C_2 symmetry for DPA in the ^{1}B S_1 excited state and no symmetry at all for the electronic ground state configuration. The long Franck–Condon progressions in the spectrum indicate a large change in the equilibrium geometry of the molecule in the $S_1\leftarrow S_0$ transition. These progressions are most pronounced in two low-frequency modes. The change will, therefore, be predominantly along those normal coordinates. Similar results have been obtained for the transition from the S_1-state to the ionic ground state.[25]

From the S_0 and S_1-state geometries and their normal modes, the Franck–Condon factors can in principle be calculated. This is however a formidable task and has not been done here. Nonetheless, a qualitative understanding of the origin of the Franck–Condon progressions can be obtained by looking at the geometry differences between the ground and excited state. From Table III we see that changes occur mainly in the relative twist of the phenyl-rings (probably best expressed by the summed torsional angles) and the pyramidality around the N-atom (expressed by the inversion angle β). The Cl-N-Cl$'$ bond angle θ, on the other hand, hardly changes. Long Franck–Condon progressions would, therefore, be expected in the modes corresponding to these geo-

TABLE VIII. Experimentally observed lines in the excitation spectrum of the first electronically excited singlet state of the DPA-Xe van der Waals complex, recorded on mass 298, 300, and 301 Da. The frequencies are given in wave numbers relative to the electronic origin of DPA-Xe at (32395.5 ± 0.3) cm^{-1}, which is (66.2 ± 0.3) cm^{-1} redshifted from the origin of DPA. The intensities are relative to the intensity of the electronic origin, which is set to 100. s denotes a shoulder. In the assignment intramolecular vibrational modes are denoted with ν_i, while ω_j denotes a van der Waals mode. A + denotes a combination band, and the mode that is expected to have the largest contribution to the line is mentioned first.

Frequency	Intensity		Mode
0.0	100		origin
24.0	23		ω_1
62.3	27		ν_1
64.7	47		ω_3
65.9	47	(s)	?
67.1	97		ν_2
68.0	71	(s)	?
68.9	34	(s)	?
87.9	19		$\omega_1 + \omega_3$
90.8	33		$\nu_2 + \omega_1$
96.4	39		ν_3
120.2	15		$\nu_3 + \omega_1$
129.2	25	(s)	$\nu_1 + \nu_2$
130.2	37		?
131.4	37		$\nu_2 + \omega_3$
132.4	42		?
133.6	42		$2\nu_2$
158.8	22		$\nu_1 + \nu_3$
160.2	32		
161.6	23		$\nu_3 + \omega_3$
164.0	33		$\nu_3 + \nu_2$
192.3	21		$2\nu_3$
195.2	25		$\nu_1 + 2\nu_2$
199.2	31		$3\nu_2$
225.2	17		$\nu_1 + \nu_3 + \nu_2$
227.1	24		$\nu_3 + \nu_2 + \omega_3$
229.7	19		$\nu_3 + 2\nu_2$

metrical parameters, i.e., in the torsional mode and/or in the umbrella mode. Note however, that the normal modes of ground and excited state DPA are not ''pure local modes'' and especially the torsional motion and the wagging motion show a strong mixing, that is different for the ground and excited state.

It is interesting to understand which motions are associated with the low-frequency modes that are most active in the electronic spectrum. All lines below 300 cm^{-1} in the spectrum of H-DPA can be attributed to 4 fundamental frequencies (ν_1, ν_2, ν_3, and ν_5 in Table I) and their overtones and combination bands. The ν_4-mode of DPA is of particular interest. This mode can not be identified in the H-DPA spectrum, however it is clearly present in the D-DPA spectrum at 198.2 cm^{-1}. A progression of overtone and combination bands is built on this mode. Interestingly, it is the only low-frequency mode for which calculations show a clear frequency shift upon deuteration. Applying this calculated shift to the experimental ν_4-value of D-DPA results in an expected ν_4-frequency of 204 cm^{-1} for H-DPA. Inspection of the H-DPA spectrum shows lines around that frequency that all could be assigned to other bands or combination bands. It

could therefore well be the case that the ν_4-progression in H-DPA is hidden under those other lines.

Three of the fundamental frequencies are found to be below 100 cm^{-1}. This is remarkably well reproduced in the calculations. The ν_1 vibrational line is hidden in the wing of the ν_2, but its overtone and combination bands with ν_2 and ν_3 can be recognized in the spectrum. The best evidence for the ν_1-mode is obtained from its clear appearance in the spectra of the vdW-complexes (see below). A further indication for its existence is inferred from a broad and weak spectral feature that is sometimes present ≈ 35 cm^{-1} *above* the electronic origin of the $S_1 \leftarrow S_0$ transition. If this feature is to be explained by a hot band transition, then it has to be a $\Delta v = 0$ transition in a mode that has a ground state frequency ≈ 35 cm^{-1} lower than the corresponding excited state frequency. As there are no hot bands observed on the red side of the DPA origin, the observed hot band most likely involves the ν_1-mode; hot bands involving the ν_2 and ν_3-modes would be expected to appear on the red side of the origin ($\Delta v = -1$) as well. As the excited state frequency of the ν_1-mode is 59.1 cm^{-1}, the corresponding ground state frequency is around 24 cm^{-1}. This number is surprisingly close to the calculated lowest frequency of the ground state of 26 cm^{-1}.

The agreement between experiment and calculation is a strong indication that the first three experimentally observed excited state frequencies can be attributed, in terms of local modes, to the ''umbrella mode'' and the in-phase phenyl-ring ''wagging'' and ''torsion'' modes (in random order). It is, however, hard to decide exactly what motion belongs to which experimental frequency. Strict symmetry arguments can not be used due to the lack of molecular symmetry in the electronic ground state. Replacing the hydrogen atom at the nitrogen with a deuterium atom does help identifying modes that involve motion of this atom. There is, however, hardly any motion of this atom in the lowest three modes.

Nevertheless, arguments can be made for the identification of the ν_1 with the ''umbrella mode.'' Clear symmetries will lead to tight selection rules, approximate symmetries may yield propensity rules. The ground state geometry has C_1 symmetry due to the pyramidal structure around the N-nucleus. Visual inspection, however, shows that the molecule has almost C_2 symmetry. We therefore would expect transitions from the vibrationless level in the S_0-state (approximate A-symmetry) to S_1-modes with A-symmetry to have larger intensity than transitions to modes with B-symmetry. In the experimental spectrum, we have one weak (ν_1) and two strong (ν_2 and ν_3) modes. This can be compared to the calculations where two of the three calculated low-frequency modes have A-symmetry while one has B-symmetry. It therefore seems likely that the ν_1-mode corresponds to the calculated 74 cm^{-1}, B-symmetry ''umbrella mode.'' In addition, overtone and combination bands of the ν_1-mode are seen to have appreciable intensity in the REMPI spectrum. This is consistently explained by the increasing amount of A character in these bands. In addition, the ν_1-mode is more clearly present in the spectra of the vdW-complexes than in spectra of uncomplexed DPA. This is due to two effects. First, the ν_1 is spectrally better resolved from

the ν_2 as a result of the frequency shifts of the modes upon complexing (see next section). Second, the C_2 symmetry of the excited state is broken in the complex, thereby making transitions to the ν_1-mode less forbidden.

The frequency ν_2 can then be identified either with the "torsion mode," or with the "wagging mode." Strongly active modes in the 60 cm^{-1} range have been observed for biphenylic species in other studies.[7–9,11] These are usually attributed to torsional motion of the phenyl rings. The experiment presented here does not give direct information on the motion involved in the ν_2-mode. On the basis of a comparison between the experimental and calculated S_1-state frequencies one might conclude in favour of the wagging mode. It is therefore difficult to decide whether the ν_2-mode corresponds to the "wagging mode" and the ν_3-mode to the torsion or vice versa and the nature of these two modes remains unclear. Further studies using isotopically substituted species might clarify this point.

B. van der Waals complexes with diphenylamine

Several modes of the complexes are assigned as van der Waals modes. An assignment of vdW-modes in terms of bending and stretching modes has been an important objective of many studies. This is difficult, however, because floppy, large amplitude motions are involved, rather than clear bending and stretching motions. This is recently pointed out in a comprehensive study on the benzene-Ar van der Waals complex.[36]

The electronic origin in all spectra are red shifted relative to the monomer. This is commonly interpreted as the rare gas atom being positioned on top of an aromatic ring.[31] An interesting observation from the spectra is the stiffening of the intra-molecular low-frequency modes upon complexing. Usually, the presence of a vdW-bonded rare gas atom does not influence the normal mode frequencies of the molecules to a large extent. A weak coupling between the modes within DPA and the vdW-modes of the rare gas atom can change the frequency of these modes, as in a system of coupled oscillators. We would expect the mode with the largest relative motion between the phenyl ring and the rare gas atom to couple most efficiently and therefore to exhibit the largest frequency shift. In the previous section we concluded that the lowest three mode frequencies involve motions of the phenyl-rings relative to the frame of the molecule. We would expect the frequency shift to differ for these three modes. Interestingly, in the vdW-complex the ν_1-mode is now clearly separated from the ν_2-mode. That is consistent with the ν_1-mode being the umbrella mode, since this mode has a lower amplitude phenyl motion than the torsion or wagging mode.

In addition to a change in frequency of the low-frequency intra-molecular vibrations, the intensity distribution in the spectra is changed as well. It is also observed that extra lines appear in the spectrum, and several hundred wave numbers above the origin individual lines can no longer be resolved. This is partly due to the change in symmetry of the excited state and the mixing of the intra-molecular modes

with the vdW-modes, but might also be due to a shorter lifetime of the S_1-state for the complex.

VI. CONCLUSIONS

Vibrationally resolved electronic spectra of diphenylamine are measured in a laser desorption jet cooling molecular beam spectrometer. The $S_1 \leftarrow S_0$ excitation spectrum of DPA is dominated by long progressions in low-frequency vibrational modes that involve the motion of the two phenyl rings relative to the frame of the molecule. *Ab initio* calculations have been performed on the geometry and the vibrational properties of DPA in both the S_0 and the S_1-state.

The calculations show that DPA changes from a pyramidal equilibrium geometry around the N-atom with unequal torsional angles of the phenyl rings around the C-N bonds (C_1 symmetry) to a planar geometry around N with equal torsional angles (C_2 symmetry) in the $S_1 \leftarrow S_0$ transition. This is the result from a ($\pi^* \leftarrow n$) electronic excitation that effectively changes the sp^3 configuration around N to a sp^2 configuration. Experiment and calculations agree on five low-frequency phenyl ring motions below 300 cm^{-1}, with three of them below 100 cm^{-1}. These three normal modes are mixtures of the local "umbrella," "in-phase ring torsion," and "in-phase ring wagging" modes, and are mixed to a different extent in the two electronic states. The lowest frequency mode in the S_1-state at 59.1 cm^{-1} is assigned to the "umbrella" or "inversion mode." The corresponding mode in the S_0-state is around 24 cm^{-1}. No clear assignment on the other two modes below 100 cm^{-1} in the S_1-state (62.1 and 89.7 cm^{-1}) can be given. Ion dip measurements are performed to probe the ground state vibrations. A mode at 51.2 cm^{-1} is found that is the counterpart of the excited state 62.1 cm^{-1} mode.

From the REMPI spectra of the van der Waals complexes of DPA with Ar, Kr, and Xe we conclude that the rare gas atom sits on top of a phenyl ring. The van der Waals modes couple with the floppy ring motions which results in a marked frequency increase of the three low-frequency modes, as well as in different intensity distributions in the spectra.

[1] R. J. W. le Fèvre and J. D. Saxby, J. Chem. Soc. B **11**, 1064 (1966).

[2] J. P. Canselier and P. Cassoux, J. Mol. Struct. **39**, 301 (1977).

[3] J. E. Adams, W. W. Mantulin, and J. R. Huber, J. Am. Chem. Soc. **95**, 5477 (1973).

[4] J. R. Huber and J. E. Adams, Ber. Bunsenges. Phys. Chem. **78**, 217 (1974).

[5] H. J. Haink, J. E. Adams, and J. R. Huber, Ber. Bunsenges. Phys. Chem. **78**, 436 (1974).

[6] H. J. Haink and J. R. Huber, Chem. Phys. Lett. **44**, 117 (1976).

[7] K. W. Holtzclaw and D. W. Pratt, J. Chem. Phys. **84**, 4713 (1986).

[8] S. Kamei, T. Sato, N. Mikami, and M. Ito, J. Phys. Chem. **90**, 5615 (1986).

[9] J. H. Frederick, E. J. Heller, J. L. Ozment, and D. W. Pratt, J. Chem. Phys. **88**, 2169 (1988).

[10] I. Baraldi, E. Gallinella, and F. Momicchioli, J. Chem. Phys. **83**, 653 (1986).

[11] R. Zimmermann, C. Weickhardt, U. Boesl, and E. W. Schlag, J. Mol. Struct. **327**, 81 (1994).

[12] N. N. Gusakova, A. N. Pankratov, E. E. Federov, S. P. Mushtakova, and L. A. Gribov, Zh. Strukt. Khim. **22**, 37 (1981); A. N. Pankratov, S. P. Mushtakova, and L. A. Gribov, *ibid*. **26**, 170 (1985); A. N. Pankratov, *ibid*. **32**, 23 (1991); Eng. Ed. J. Struct. Chem. **32**, 177 (1991).

[13] V. B. Luzhkov and T. N. Yakushchenko, Zh. Strukt. Khim. **31**, 30 (1990); Eng. Ed. J. Struct. Chem. **31**, 24 (1990).

[14] S. Quillard, G. Louarn, J. P. Buisson, S. Lefrant, J. Masters, and A. G. MacDiarmid, Synth. Met. **49-50**, 525 (1992).

[15] A. Ito, K. Ota, K. Yoshizawa, K. Tanaka, and T. Yamabe, Chem. Phys. Lett. **223**, 27 (1994).

[16] C. Brassy and J. P. Mornon, Compt. Rend. Acad. Sci. (Paris) C **274**, 1728 (1972).

[17] A. Mellier and C. Brassy, Compt. Rend. Acad. Sci. (Paris) B **276**, 177 (1973).

[18] J. P. Mornon, R. Bally, and C. Brassy, Compt. Rend. Acad. Sci. (Paris) C **284**, 779 (1977).

[19] T. Kobayashi and S. Koshihara, Chem. Phys. Lett. **104**, 174 (1984).

[20] R. Rahn, J. Schroeder, J. Troe, and K. H. Grellmann, J. Phys. Chem. **93**, 7841 (1989).

[21] D. H. Levy, Science **214**, 263 (1981).

[22] *Atomic and Molecular Beam Methods*, edited by G. Scoles (Oxford University Press, Oxford, 1988).

[23] G. Meijer, M. S. de Vries, H. E. Hunziker, and H. R. Wendt, Appl. Phys. B **51**, 395 (1990).

[24] M. G. H. Boogaarts and G. Meijer, J. Chem. Phys. **103**, 5269 (1995).

[25] M. G. H. Boogaarts, P. C. Hinnen, and G. Meijer, Chem. Phys. Lett. **223**, 537 (1994).

[26] M. G. H. Boogaarts and G. Meijer, Rev. Sci. Instrum. (in preparation).

[27] S. Gerstenkorn and P. Luc, *Atlas du Spectroscopie d'Absorption de la Molecule d'Iode* (CNRS, Paris, 1978); Rev. Phys. Appl. **14**, 791 (1979).

[28] D. E. Cooper, C. M. Klimcak, and J. E. Wessel, Phys. Rev. Lett. **46**, 324 (1981).

[29] J. Murakami, K. Kaya, and M. Ito, Chem. Phys. Lett. **91**, 401 (1982).

[30] C. E. Hamilton, J. L. Kinsey, and R. W. Field, Annu. Rev. Phys. Chem. **37**, 493 (1986).

[31] For a review see, e.g., P. Hobza, H. L. Selzle, and E. W. Schlag, Chem. Rev. **94**, 1767 (1994).

[32] M. J. Frisch, G. W. Trucks, H. B. Schlegel, P. M. W. Gill, B. G. Johnson, M. A. Robb, J. R. Cheeseman, T. A. Keith, G. A. Petersson, J. A. Montgomery, K. Raghavachari, M. A. Al-Laham, V. G. Zakrzewski, J. V. Ortiz, J. B. Foresman, J. Cioslowski, B. B. Stefanov, A. Nanayakkara, M. Challacombe, C. Y. Peng, P. Y. Ayala, W. Chen, M. W. Wong, J. L. Andres, E. S. Replogle, R. Gomperts, R. L. Martin, D. J. Fox, J. S. Binkley, D. J. Defrees, J. Baker, J. P. Stewart, M. Head-Gordon, C. Gonzalez, and J. A. Pople, GAUSSIAN 94 (Revision B.3), Gaussian, Inc., Pittsburgh, Pennsylvania, 1995.

[33] G. Herzberg, *Molecular Spectra and Molecular Structure* (Van Nostrand Reinhold, New York, 1945), Vol. 2, p. 439.

[34] B. Kleibömer and D. H. Sutter, Z. Naturforsch. **43a**, 561 (1988).

[35] G. Meijer, G. Berden, W. L. Meerts, H. E. Hunziker, M. S. de Vries, and H. R. Wendt, Chem. Phys. **163**, 209 (1992).

[36] E. Riedle, R. Sussmann, Th. Weber, and H. J. Neusser, J. Chem. Phys. **104**, 865 (1996); E. Riedle and A. van der Avoird, *ibid*. **104**, 882 (1996).